Inorganic Chemistry

Article

pubs.acs.org/IC

Formation of Crystalline $Na_2V_6O_{16}\cdot 3H_2O$ Ribbons into Belts and Rings

P. Chithaiah,[†] G. T. Chandrappa,*[,†] and J. Livage[‡]

[†]Department of Chemistry, Central College, Bangalore University, Bangalore 560001, India

[‡]Chimie de la Matiere Condensee, College de France, 11 place Marcelin Berthelot, 75231 Paris, France

ABSTRACT: Single-crystalline nanobelts and nanorings of $Na_2V_6O_{16}\cdot 3H_2O$ structures have been facilely synthesized through a direct hydrothermal reaction between $NaVO_3$ and H_3PO_4, without the addition of any harmful solvents or surfactants. The analytical techniques of scanning electron microscopy, transmission electron microscopy (TEM), powder X-ray diffraction, thermogravimetric analysis, energy-dispersive X-ray spectroscopy, Fourier transform infrared, high-resolution TEM, and selected-area electron diffraction have been used to characterize the morphology, composition, and structure of the synthesized products. The $Na_2V_6O_{16}\cdot 3H_2O$ nanobelts are up to several hundreds of micrometers in length and 100−300 nm in thickness, and for nanorings, the diameters are 4.5−6.5 μm. H_3PO_4 plays a key role in maintaining the pH of the solution as well as producing PO_4^{3-} ions in solution. The chemical reactions and a possible growth mechanism involved in the formation of $Na_2V_6O_{16}\cdot 3H_2O$ nanobelts and nanorings are briefly discussed.

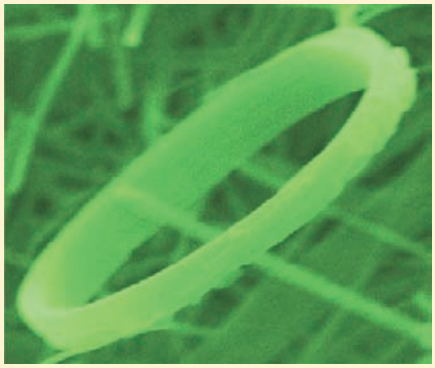

INTRODUCTION

The synthesis of nanostructured materials with well-controlled size, morphology, and chemical composition has been of great interest because their novel physical and chemical properties.[1] Among them, vanadium oxide based nanostructured materials show mainly rich chemistry because of the variable vanadium oxidation state and its flexible coordination environment.[2] A rich diversity of vanadium oxide bronzes and intercalation compounds based on the incorporation of either alkali or transition metals within the interstitial spaces of the vanadium oxide tunnel framework has been extensively studied.[3] Among them, alkali-metal or alkaline-earth metal vanadium oxide bronze-hydrated compounds ($M_2V_6O_{16}\cdot nH_2O$, where M = Na and K, or $MV_6O_{16}\cdot nH_2O$, where M = Mg and Ca) have been widely studied during the past decade. They find extensive applications in areas such as high-energy lithium batteries, heterogeneous catalysis, photochromism, electrochromism, and chemical sensors.[4−12]

Several synthetic routes such as microemulsion-mediated systems, arc discharge, laser-assisted catalysis growth, solution, vapor transport, and solvothermal and hydrothermal methods have been successfully explored to fabricate various kinds of nanostructured vanadium oxides and their derived compounds. As one of the solution methods, the hydrothermal method has been extensively used for the synthesis of inorganic compounds. A large family of trivanadate and hexavanadate phases have been synthesized under the hydrothermal process.[13−15] However, to the best of our knowledge, there have been few literature examples on the synthesis of $Na_2V_6O_{16}\cdot 3H_2O$ nanostructures.[16−18]

The importance of sodium hexavanadates has strongly increased because of the specific charge and magnetic ordering associated with mixed-valence states in these compounds.[19]

Previously, various kinds of vanadium oxide nanostructures such as nanowires, nanobelts, nanorods, nanotubes, nanostructured foam, nanoribbons, and rose-like nanostructures have been reported.[20,21] However, presently, it has been demonstrated that several new geometrical configurations such as nanosprings,[22] nanorings,[22−24] and nanohelices[25,26] grown from 1D nanobelts/fibers or nanoribbons are of special interest because of their structural flexibility, size, and special morphology-related properties. Nanorings, in particular, show many unusual behaviors, receive an abnormal dispersion of magnetic field in semiconductor nanorings, and motivate much interest in the theoretical and experimental study of the electronic and optical properties because of three-dimensional topological quantum effects for electrons confined in nanorings.[27,28] This has motivated our current research. For instance, Shen and Chen reported on the discovery of $Ag_2V_4O_{11}$ nanorings and microloops.[23] Liu and Xue reported the formation of $V_2O_5\cdot xH_2O$ nanorings and microloops.[24] More recently, we reported $(NH_4)_{0.5}V_2O_5\cdot mH_2O$ ring/triangle and oval forms.[20] To the best of our knowledge, the $Na_2V_6O_{16}\cdot 3H_2O$ nanorings have never been reported in the literature. Herein, we report for the first time that the $Na_2V_6O_{16}\cdot 3H_2O$ nanorings have been synthesized by hydrothermal treatment (HTT) upon acidification of $NaVO_3$ with H_3PO_4 without the use of any harmful solvents or surfactants.

EXPERIMENTAL SECTION

Chemical reagents of analytical grade were purchased from Merck Ltd. and used as received without further purification. Double-distilled water was used throughout the experiments. $Na_2V_6O_{16}\cdot 3H_2O$

Received: October 18, 2011
Published: February 7, 2012

   dx.doi.org/10.1021/ic202260w | *Inorg. Chem.* 2012, 51, 2241−2246

nanorings were prepared via a hydrothermal technique in a Teflon-lined stainless steel autoclave. A typical procedure following the synthesis of $Na_2V_6O_{16}\cdot 3H_2O$ nanorings is described as follows. A total of 0.25 g of sodium metavanadate (2.05×10^{-3} mol; $NaVO_3$) powder was added to 15 mL of distilled water taken in a 20-mL Teflon tube. The pH of the solution was adjusted to ~2.0 by adding 3 drops of orthophosphoric acid (H_3PO_4, 88%) using a 2-mL pipet, resulting in the formation of a wine-red solution, and stirred for 15 min. Subsequently, the wine-red solution was filled into Teflon-lined stainless steel autoclaves. The autoclaves were maintained at variable temperatures for different durations. Once the HTT was completed, the autoclaves were cooled to ambient temperature naturally. The reddish-brown nonadherent spongelike bulk material was collected and washed with distilled water, followed by ethanol several times. The final product was dried in an oven at 60 °C for 2 h.

Characterization. Powder X-ray diffraction (PXRD) data were recorded on a Philips X'pert PRO X-ray diffractometer with graphite-monochromatized Cu Kα radiation (λ = 1.541 Å) operated at 40 kV and 30 mA. The Fourier transform infrared (FTIR) spectrum of the sample was collected using a Thermo Nicolet FTIR spectrometer. The water content in the sample was investigated by thermogravimetric analysis (TGA) using a SDT Q600 thermomicrobalance in a N_2 atmosphere from room temperature to 600 °C at a heating rate of 10 °C min^{-1}. The morphologies of the products were examined by a Quanta-200 scanning electron microscope equipped with an energy-dispersive X-ray spectroscope. Samples were gold-coated prior to scanning electron microscopy (SEM) analysis. The nano/microstructure of the products was observed by transmission electron microscopy (TEM) and selected-area electron diffraction (SAED), which was performed with a Hitachi model H-600 instrument operating at 100 kV. High-resolution TEM (HRTEM) images were taken with a JEOL 3011, 300 kV instrument with an ultrahigh-resolution pole piece.

RESULTS AND DISCUSSION

Figure 1 shows the PXRD pattern of the as-synthesized product. All of the diffraction peaks in the pattern can be

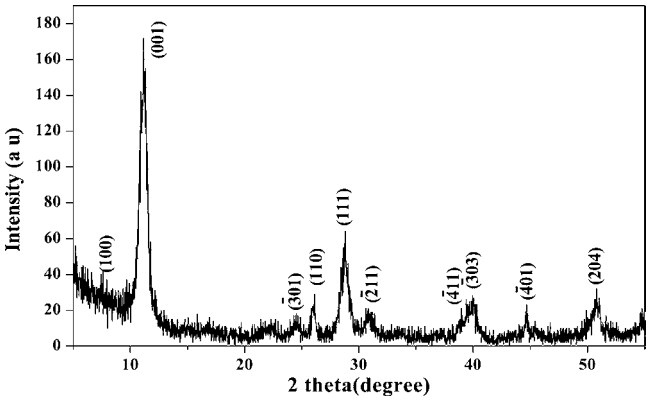

Figure 1. PXRD pattern of the $Na_2V_6O_{16}\cdot 3H_2O$ product.

indexed to a pure monoclinic crystalline phase of $Na_2V_6O_{16}\cdot 3H_2O$ (according to JCPDS No. 16-601 for $Na_2V_6O_{16}\cdot 3H_2O$). No reflections of impurity were found in the pattern, which proves that pure $Na_2V_6O_{16}\cdot 3H_2O$ has been successfully synthesized. The basal distance for a strong (001) peak is 7.87 Å, which matches well with a previously reported value.[18]

Figure 2 shows the FTIR spectrum of the as-synthesized product. The absorption bands between 400 and 1001 cm^{-1} can be indexed to various vibrational modes of the V−O groups. The bands located at 535 and 826 cm^{-1} are attributed to the symmetric and asymmetric vibrational modes of V−O−V stretching vibrations, respectively. The two main absorption bands at 1001 and 964 cm^{-1} are respectively assigned to the stretching vibrations of V^{5+}=O and V^{4+}=O groups, corresponding to the existence of the short-range order of the VO_6 unit. The band at 728 cm^{-1} is ascribed to a V−OH_2 stretching mode due to coordinated water.[29] The band located at 1626 cm^{-1} is related to the bending vibrations of the O−H groups of water molecules.[30]

Figure 3 shows the TGA curve of the as-synthesized $Na_2V_6O_{16}\cdot 3H_2O$ product. The TGA profile shows a weight loss of 7.9% from 100 to 360 °C, corresponding to the removal of adsorbed water molecules. This value matches well with the water content (8.16%) of the $Na_2V_6O_{16}\cdot 3H_2O$ sample. The results from PXRD, FTIR, and TGA studies confirmed that the product is $Na_2V_6O_{16}\cdot 3H_2O$.

The morphology of the as-synthesized $Na_2V_6O_{16}\cdot 3H_2O$ nanostructures at different temperatures was investigated by SEM. Parts A−E of Figure 4 show the representative SEM images of the as-synthesized $Na_2V_6O_{16}\cdot 3H_2O$ nanostructures with different magnifications. When the temperature is maintained at 130 °C for 24 h, as shown in Figure 4A, the reddish-brown product exhibits flexible beltlike morphology. After 48 h, as observed in a low-magnification SEM image (Figure 4B), one can observe that the resulting product reveals a large amount of flexible beltlike nanostructures with typical lengths up to several hundreds of micrometers in addition to a significant amount of nanorings. Parts C−E of Figure 4 show the selective high-magnification SEM images of the interesting $Na_2V_6O_{16}\cdot 3H_2O$ nanorings obtained at 130, 150, and 180 °C for 48 h, respectively. It is found that all of the $Na_2V_6O_{16}\cdot 3H_2O$ nanorings are perfectly circular with uniform shapes and flat surfaces. Typical nanorings have diameters of 4.5−6.5 μm with a thickness of 100−300 nm, respectively. The process is of high reproducibility from run to run, and the yield of nanorings is relatively not very high. The energy-dispersive X-ray spectroscopy (EDX) spectrum (Figure 4F) was measured to determine the chemical composition of the $Na_2V_6O_{16}\cdot 3H_2O$ sample. The spectrum exhibits the characteristic sodium, vanadium, and oxygen absorption peaks (hydrogen cannot be detected by EDX).

The detailed morphology and structure of $Na_2V_6O_{16}\cdot 3H_2O$ nanobelts/rings was further characterized by TEM and HRTEM. The TEM image (Figure 5A) shows that the width and thickness of the nanobelts are in the range of 200−300 and 100−200 nm, respectively. Figure 5B shows the TEM image of $Na_2V_6O_{16}\cdot 3H_2O$ nanobelts/rings. From the HRTEM image shown in Figure 5C, it is found that the distance between neighboring planes is ~7.81 Å. This distance is consistent with the (001) plane of the monoclinic $Na_2V_6O_{16}\cdot 3H_2O$ structure, as observed in the PXRD pattern, which shows that these nanobelts/rings grow along the (001) direction. The SAED pattern (Figure 5D) taken from an individual nanobelt/ring can be attributed to monoclinic $Na_2V_6O_{16}\cdot 3H_2O$ nanostructures, indicating that the nanobelts and nanorings are structurally uniform and a good single-crystal structure.

The chemical reactions involved in the formation of $Na_2V_6O_{16}\cdot 3H_2O$ nanobelts/rings can be formulated as follows:

$$3NaVO_3 + H_3PO_4 \xrightarrow{\text{room temperature}} 3VO_3^- + Na_3PO_4 + 3H^+ \ldots \quad (1)$$

dx.doi.org/10.1021/ic202260w | Inorg. Chem. 2012, 51, 2241−2246

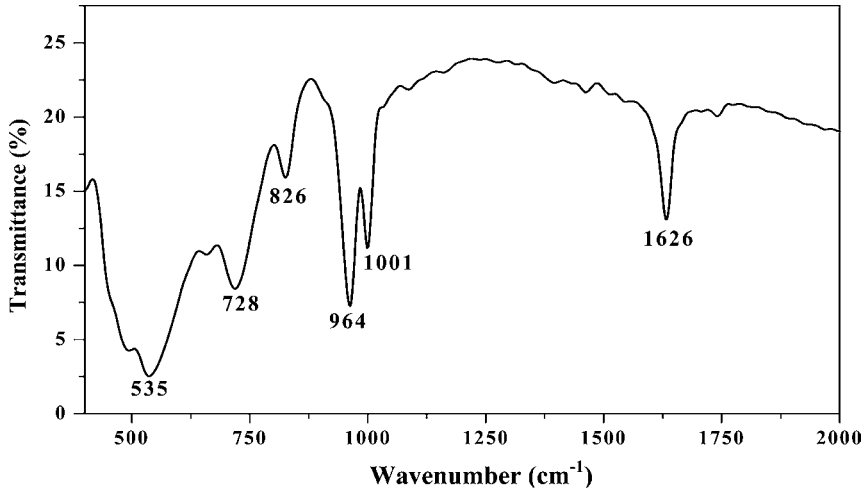

Figure 2. FTIR spectrum of the $Na_2V_6O_{16}\cdot 3H_2O$ product.

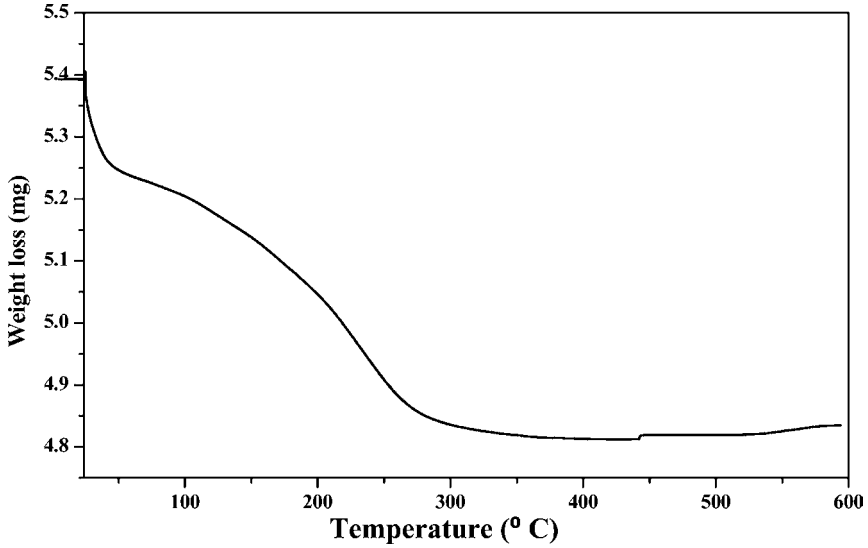

Figure 3. TGA curve of the $Na_2V_6O_{16}\cdot 3H_2O$ product.

$$11VO_3^- + 8H^+ + H_2O \xrightarrow{\text{room temperature}} [H_2V_{10}O_{28}]^{4-} + [VO_2(H_2O)_4]^+ \ldots \quad (2)$$

$$[H_2V_{10}O_{28}]^{4-} + 4H^+ + 32H_2O \xrightarrow{\text{HTT}} 10[VO(OH)_3(H_2O)_2] \ldots \quad (3)$$

$$[VO_2(H_2O)_4]^+ \xrightarrow{\text{HTT}} [VO(OH)_3(H_2O)_2] + H^+ \ldots \quad (4)$$

$$6[VO(OH)_3(H_2O)_2] + 2Na^+ \xrightarrow{\text{HTT}} Na_2V_6O_{16}3H_2O + 17H_2O + 2H^+ \ldots \quad (5)$$

In this process, sodium metavanadate in aqueous solution forms Na^+ and VO_3^-. Acidification of VO_3^- with H_3PO_4 leads to the formation of a wine-red solution of vanadic acid (HVO_3, pH ≈ 2), as shown in eq 1. The HVO_3 solution then progressively gets converted into a mixture of decavanadate $[H_2V_{10}O_{28}]^{4-}$ and $[VO_2(H_2O)_4]^+$ ions (shown in eq 2), which has been observed previously by ^{51}V NMR spectroscopy.[16] The resulting solution was subjected to HTT. At the early stage of HTT, we could expect that the decavanadate $[H_2V_{10}O_{28}]^{4-}$ species gets protonated (eq 3) and the cationic $[VO_2(H_2O)_4]^+$ species undergoes deprotonation (eq 4) in order to provide neutral $[VO(OH)_3(H_2O)_2]$ precursors. It is well-known that the composition of the V^{5+} solution changes with the pH. According to the so-called partial charge model,[32] a vanadate solution of pH > 1 should contain a mixture of a neutral species $[VO(OH)_3(H_2O)_2]$ and a negatively charged precursor $[VO(OH)_4(H_2O)]^-$. Therefore, the hydrated sodium hexavanadate $Na_2V_6O_{16}\cdot 3H_2O$ phase results from polycondensation of these precursors in the presence of Na^+ ions, leading to the formation of $V_6O_{16}^{2-}$ layers, and the hydrated Na^+ ions can accommodate within these $V_6O_{16}^{2-}$ framework tunnels in order to compensate for the negative charge of the layers, in a manner similar to that previously proposed for the formation of $Na[V_3O_8]$.[16,32]

Growth Mechanism. The growth mechanism for the formation of nanorings of vanadium oxide based materials can be understood on the basis of their layered structures. For example, Shen and Chen proposed the loop-by-loop coaxial, uniradius, self-coiling of a single nanobelt in order to explain

dx.doi.org/10.1021/ic202260w | Inorg. Chem. 2012, 51, 2241−2246

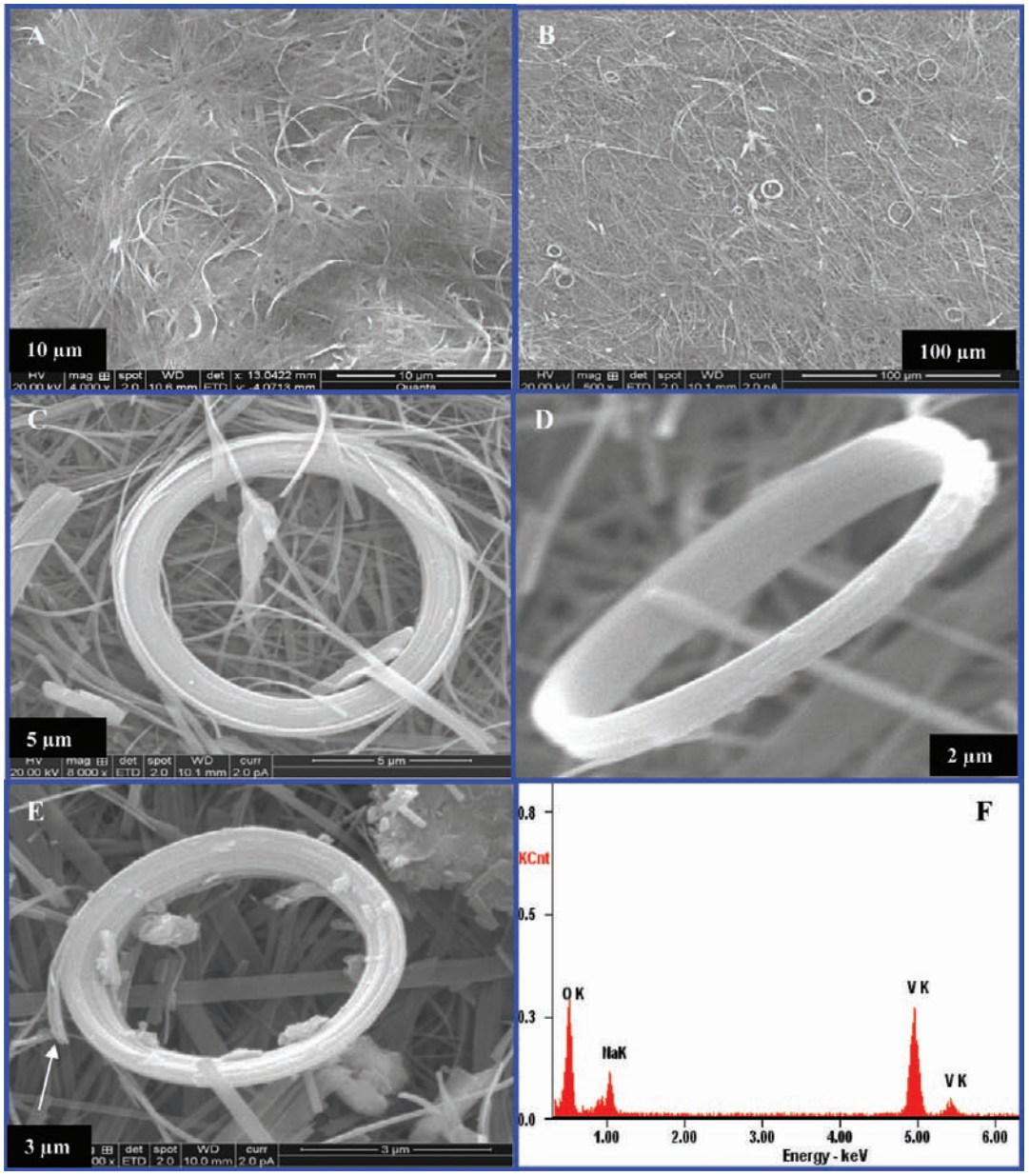

Figure 4. SEM images of the $Na_2V_6O_{16}\cdot 3H_2O$ product synthesized at different temperatures: (A) 130 °C, 24 h; (B,C) 130 °C, 48 h; (D) 150 °C, 48 h; (E) 180 °C, 48 h. (F) EDX spectrum of $Na_2V_6O_{16}\cdot 3H_2O$.

the formation of $Ag_2V_4O_{11}$ nanorings and microloops from solutions,[23] in a manner similar to that proposed previously for the formation of ZnO nanorings in the vapor phase.[31] A "cation induced coiling growth mechanism" was suggested by Liu and Xue to describe the formation of $V_2O_5\cdot xH_2O$ nanorings and microloops. In a recent publication, we suggested a similar process for the formation of $(NH_4)_{0.5}V_2O_5\cdot mH_2O$ rings, triangles, and ovals from solutions and proposed that these were formed when two ends of a belt connect through the edge- and corner-sharing of VO_5 square pyramids. However, the exact mechanism for the formation of $Na_2V_6O_{16}\cdot 3H_2O$ nanostructures is still unclear. It is well-known that the $Na_2V_6O_{16}\cdot 3H_2O$ phase cannot result from a solid-state transformation, and then the structural transformation should involve a redissolution−precipitation process under the hydrothermal process. Previously, Yu and Zhou groups have synthesized $Na_2V_6O_{16}\cdot 3H_2O$ nanobelts and nanowires in the presence of F^- and SO_4^{2-} anions, respectively.[17,18] They suggested that the anions are crucial for the formation of $Na_2V_6O_{16}\cdot 3H_2O$ nanobelts and nanowires. Therefore, in the present work, we could expect that H_3PO_4 plays an important role because of its polar nature, high solubility in water, and dissociation into H^+ and PO_4^{3-} ions in the solution. The H^+ ions maintain the pH of the solution (pH ≈ 2). With the support of the F^- and SO_4^{2-} anions, we believe that the PO_4^{3-} anions are crucial for the growth of $Na_2V_6O_{16}\cdot 3H_2O$ nanobelts because PO_4^{3-} has a stronger coordination ability than F^- and SO_4^{2-} anions and may adsorb selectively to the special crystal facets, leading to the formation of flexible $Na_2V_6O_{16}\cdot 3H_2O$ nanobelts.

The formation of $Na_2V_6O_{16}\cdot 3H_2O$ nanorings can also be explained in a manner similar to that previously proposed for the formation of $V_2O_5\cdot xH_2O$. The $Na_2V_6O_{16}\cdot 3H_2O$ structure consists of $V_6O_{16}^{2-}$ layers, and hydrated Na^+ ions are

dx.doi.org/10.1021/ic202260w | Inorg. Chem. 2012, 51, 2241−2246

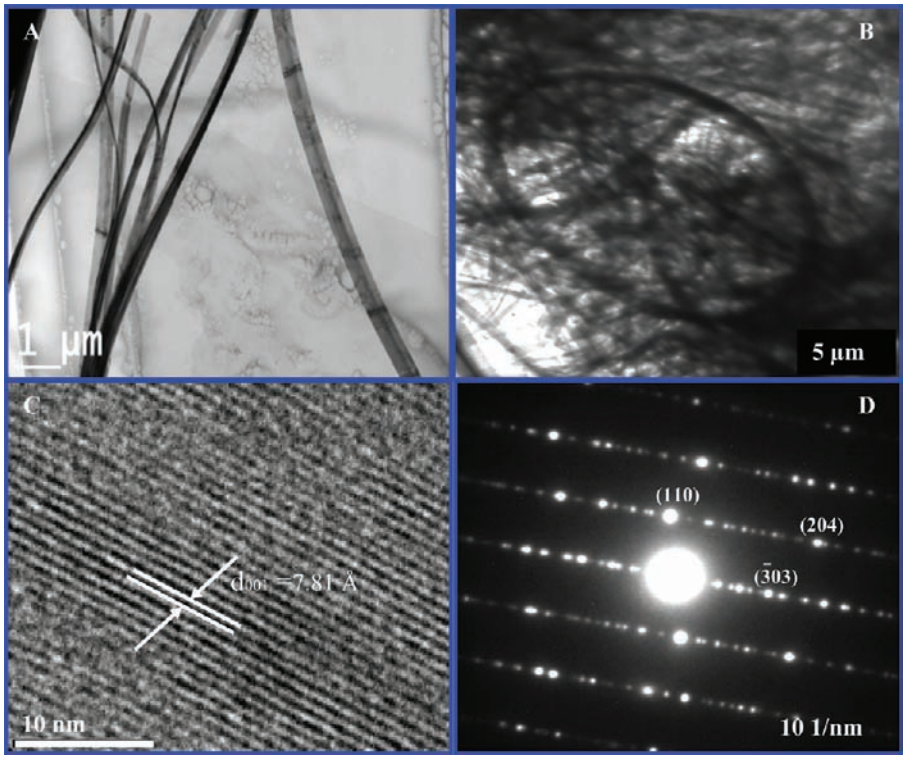

Figure 5. Representative TEM images of (A) nanobelts and (B) nanorings of $Na_2V_6O_{16}\cdot 3H_2O$. (C) HRTEM images and (D) SAED patterns of individual $Na_2V_6O_{16}\cdot 3H_2O$ nanobelts/rings.

intercalated between these layers in order to compensate for the negative charge of the layers. The V_6O_{16} layers are made of VO_6 octahedra and the V_2O_8 units of edge-sharing square pyramids. A "cation induced coiling" model should be involved in the formation of $Na_2V_6O_{16}\cdot 3H_2O$ nanorings, owing to the presence of residual or nonintercalated Na^+ ions from the solution under the hydrothermal process. According to the so-called "cation induced coiling" model, we may assume that the nonintercalated Na^+ ions can be adsorbed by the $V{=}O^{\delta-}$ dipoles on both sides of the $Na_2V_6O_{16}\cdot 3H_2O$ nanobelt. When the amount of Na^+ ions adsorb asymmetrically on both the top or bottom surfaces of a thin, straight $Na_2V_6O_{16}\cdot 3H_2O$ nanobelt, an asymmetric strain energy is induced. When this asymmetric-induced strain energy becomes larger than the elasticity energy, the straight $Na_2V_6O_{16}\cdot 3H_2O$ nanobelt tends to self-coil into a circular ring. The overlapping end of the belt is clearly observed in the SEM image of Figure 4E (shown by an arrowhead), which suggests the possible self-coiling of a single nanobelt into rings. However, the detailed formation mechanism of $Na_2V_6O_{16}\cdot 3H_2O$ rings might require further investigation.

CONCLUSION

In conclusion, the monoclinic phases of single-crystalline $Na_2V_6O_{16}\cdot 3H_2O$ nanorings/belts have been synthesized using a simple and environmentally friendly hydrothermal method at different temperatures without the addition of any harmful solvents or surfactants. These single-crystalline $Na_2V_6O_{16}\cdot 3H_2O$ nanorings might find applications in catalysis, nanoscale electronics, optoelectronics, and biochemical-sensing devices. The chemical reactions and a possible growth mechanism involved in the formation of $Na_2V_6O_{16}\cdot 3H_2O$ were discussed. The simple and efficient synthesis route proposed herein is presumed to be applicable to the synthesis of other metal vanadium oxide nanorings.

AUTHOR INFORMATION

Corresponding Author

*E-mail: gtchandrappa@yahoo.co.in. Phone: +91 80 22961350. Fax: +91 80 22100187.

Notes

The authors declare no competing financial interest.

ACKNOWLEDGMENTS

G.T.C. gratefully acknowledges the Department of Science and Technology, NSTI phase-IV, Government of India (GOI), for financial support. P.C. is thankful to Bangalore University for the award of a Fellowship to carry out this work.

REFERENCES

(1) Pan, Z. W.; Dai, Z. R.; Wang, Z. L. *Science* **2001**, *291*, 1947.
(2) Cao, J.; Musfeldt, J. L.; Mazumdar, S.; Chernova, N. A.; Whittingham, M. S. *Nano Lett.* **2007**, *7*, 2351.
(3) Patridge, C. J.; Jaye, C.; Zhang, H.; Marschilok, A. C.; Fischer, D. A.; Takeuchi, E. S.; Banerjee, S. *Inorg. Chem.* **2009**, *48*, 3145.
(4) Livage, J. *Chem. Mater.* **1991**, *3*, 578.
(5) Sun, X.; Li, Y. *Angew. Chem., Int. Ed.* **2004**, *116*, 3915.
(6) Poizot, P.; Grugeon, S.; Dupont, L.; Tarascon, J. M. *Nature* **2000**, *407*, 496.
(7) Liu, J.; Wang, Y.; Peng, Q.; Li, Y. *Adv. Mater.* **2005**, *17*, 764.
(8) Livage, J.; Ganguli, D. *Sol. Energy Mater. Sol. Cells* **2001**, *68*, 365.
(9) Whittingham, M. S. *Chem. Rev.* **2004**, *104*, 4271.
(10) Cao, A. M.; Hu, J. S.; Liang, H. P.; Wan, L. J. *Angew. Chem., Int. Ed.* **2005**, *44*, 4391.
(11) Whittingham, M. S.; Song, Y.; Lutta, S.; Zavalij, P. Y.; Chernova, N. A. *J. Mater. Chem.* **2005**, *15*, 3362.
(12) Wang, Y.; Cao, G. *Chem. Mater.* **2006**, *18*, 2787.

(13) Oka, Y.; Yao, T.; Yamamoto, N.; Tamada, O. *Mater. Res. Bull.* **1997**, *32*, 59.
(14) Oka, Y.; Yao, T.; Yamamoto, N. J. *Solid State Chem.* **1995**, *117*, 407.
(15) Kong, L. F.; Shao, M. W.; Xie, Q.; Liu, J. W.; Qian, Y. T. *J. Cryst. Growth* **2004**, *260*, 435.
(16) Durupthy, O.; Steunou, N.; Coradin, T.; Maquet, J.; Bonhomme, C. J.; Livage, J. *Mater. Chem.* **2005**, *15*, 1090.
(17) Yu, J. G.; Yu, J. C.; Ho, W. K.; Wu, L.; Wang, X. C. *J. Am. Chem. Soc.* **2004**, *126*, 3422.
(18) Zhou, G. T.; Wang, X. C.; Yu, J. C. *Cryst. Growth Des.* **2005**, *5*, 969.
(19) Subba Reddy, Ch. V.; Yeo, I. H.; Mho, S. I. *J. Phys. Chem. Solids* **2008**, *69*, 1261.
(20) Chandrappa, G. T.; Chithaiah, P.; Ashoka, S.; Livage, J. *Inorg. Chem.* **2011**, *50*, 7421.
(21) Chandrappa, G. T.; Steunou, N.; Livage, J. *Nature* **2002**, *416*, 702.
(22) Kong, X. Y.; Ding, Y.; Yang, R. S.; Wang, Z. L. *Science* **2004**, *303*, 1348.
(23) Shen, G. Z.; Chen, D. *J. Am. Chem. Soc.* **2006**, *128*, 11762.
(24) Liu, J.; Xue, D. *Nanoscale Res. Lett.* **2010**, *5*, 1619.
(25) Yu, D.; Wu, J. Q.; Gu, Q.; Park, H. K. *J. Am. Chem. Soc.* **2006**, *128*, 8148.
(26) Nath, M.; Parkinson, B. A. *J. Am. Chem. Soc.* **2007**, *129*, 11302.
(27) Ming, L.; Fengyu, K.; Yunxia, Z.; Li, G. *Cryst. Eng. Comm.* **2011**, *13*, 2204.
(28) Haft, D.; Schulhauser, C.; Govorov, A. O.; Warburton, R. J.; Karrai, K.; Garcia, J. M.; Schoenfeld, W.; Petroff, P. M. *Phys. E* **2002**, *13*, 165.
(29) Azambre, B.; Hudson, M. J.; Heintz, O. J. *Mater. Chem.* **2003**, *13*, 385.
(30) Sediri, F.; Gharbi, N. J. *Phys. Chem. Solids* **2007**, *68*, 1821.
(31) Kong, X. Y.; Ding, Y.; Yang, R. S.; Wang, Z. L. *Science* **2004**, 303.
(32) Durupthy, O.; Maquet, J.; Bonhomme, C.; Coradin, T.; Livage, J.; Steunou, N. J. *Mater. Chem.* **2008**, *18*, 3702.